Research Article Vol. 15, No. 3 / 1 Mar 2024 / Biomedical Optics Express 1553
Biomedical Optics EXPRESS

Comb spectroscopy of CO_2 produced from microbial metabolism

JOSHUA A. WHITAKER-LOCKWOOD,[1] SARAH K. SCHOLTEN,[1,2,*] FAISAL KARIM,[1] ANDRÉ N. LUITEN,[1,2] AND CHRISTOPHER PERRELLA[1,2,3]

[1]*Institute for Photonics and Advanced Sensing, School of Physical Sciences, University of Adelaide, Adelaide, South Australia, 5005, Australia*
[2]*ARC Centre of Excellence in Optical Microcombs for Breakthrough Science (COMBS), University of Adelaide, Adelaide, South Australia, 5005, Australia*
[3]*Centre of Light for Life and School of Biological Sciences, University of Adelaide, Adelaide, South Australia, 5005, Australia*
[*]*sarah.scholten@adelaide.edu.au*

Abstract: We have developed a direct frequency comb spectroscopy instrument, which we have tested on *Saccharomyces cerevisiae* (baker's yeast) by measuring its CO_2 output and production rate as we varied the environmental conditions, including the amount and type of feed sugar, the temperature, and the amount of yeast. By feeding isotopically-enhanced sugar to the yeast, we demonstrate the capability of our device to differentiate between two isotopologues of CO_2, with a concentration measurement precision of 260 ppm for $^{12}C^{16}O_2$ and 175 ppm for $^{13}C^{16}O_2$. We also demonstrate the ability of our spectrometer to measure the proportion of carbon in the feed sugar converted to CO_2, and estimate the amount incorporated into the yeast biomass.

1. Introduction

Human breath analysis techniques offer non-invasive methods of diagnosing diseases, tracking patient health, and monitoring the concentration of environmental contaminants in the body [1–3]. The human breath largely comprises atmospheric molecules such as CO_2 and N_2, but also contains hundreds of volatile organic compounds (VOCs) in concentrations down to the parts-per-trillion [4–7]. Some of these VOCs have been identified as biomarkers of human health and may indicate failure of bodily functions and the presence of certain diseases, depending on the concentration and type of molecule. To monitor the concentration and chemical species of these biomarkers in trace quantities requires highly sensitive and specific instrumentation that can perform measurements *in situ* and in real-time, without the need for sample storage and preparation [4,8,9]. Furthermore, an ideal breath analysis instrument should be able to distinguish between different molecules and their isotopologues, and be able to monitor a broad range of biomarkers simultaneously and continuously over long monitoring periods.

Human breath analysis has previously been performed with Gas Chromatography, and later Mass Spectrometry (GC-MS) to detect the trace-level VOCs in human breath [10–14]. GC-MS can achieve parts-per-trillion (ppt) level sensitivity and can detect many molecular species simultaneously, but is a multi-stage process requiring collection, storage, and pre-concentration, which requires substantial time and technical expertise [4,15–18]. Proton Transfer Reaction Mass Spectrometry (PTR-MS), by contrast, can be conducted in real-time while possessing a similar level of sensitivity to GC-MS techniques [9,19–22]. Recently, PTR-MS has been successfully used to monitor the breath of patients post-surgery and is also capable of detecting anaesthetic gas several weeks after an operation [23]. However, the cations used in PTR-MS do not react with all molecular species and hence other species of cations are needed for near-universal VOC detection [1,7,24]. Selected-Ion-Flow-Tube Mass Spectrometry (SIFT-MS) is a similar technique

#515988 https://doi.org/10.1364/BOE.515988
Journal © 2024 Received 14 Dec 2023; revised 26 Jan 2024; accepted 30 Jan 2024; published 12 Feb 2024

Biomedical Optics EXPRESS

to PTR-MS but where the protons are supplied by several different cation species in a fast flow tube [9,25–28]. SIFT-MS can be used to analyse a range of VOCs in real time with comparable sensitivity to PTR-MS and GC-MS [1,29–31]. However, both PTR-MS and SIFT-MS possess the key problems that GC-MS faces, such as a high instrument cost, limited miniaturisation potential, and required expertise to operate.

Laser spectroscopy is an ideal tool for human breath analysis. Unlike previously mentioned techniques, laser absorption spectroscopy probes ro-vibrational transitions of molecules that are dependent upon both the atomic weights of the molecular constituents as well as the bonds between them [32–34]. This gives laser based spectroscopy unparalleled ability to distinguish between different types of molecules and isotopes thereof. The specificity of laser absorption spectroscopy has been shown to closely match MS-based techniques and are considered a potential alternative in several applications [2,35–38]. For example, tunable diode laser absorption spectroscopy (TDLAS) can produce high resolution lineshape information to extract thermodynamic properties of the gas and differentiate between molecular species [2,4]. An optical cavity can be used in conjunction with TDLAS to increase the interaction length between the sample gas and the light to improve concentration sensitivity [2,4]. These single frequency laser sources provide ease of use, however they cannot monitor multiple molecular species simultaneously; for this a broadband light source is required.

Our aim is to develop an instrument that simultaneously exhibits some key characteristics: high sensitivity, distinguishes between different molecules and their isotopologues, and ability to monitor a broad range of biomarkers simultaneously over long periods. The instrument is based around an optical frequency comb (OFC) [39–42] with its characteristic spectrum of hundreds of evenly-spaced frequency modes over a broad frequency range. It is this combination of broad spectral coverage with numerous modes that confers the molecular specificity and sensitivity. The frequency, f_n, of each mode is given by:

$$f_n = f_0 + nf_{rep} \tag{1}$$

where f_0 is the frequency zero-offset, n is the mode number, and f_{rep} is the repetition frequency, being the difference in frequency between adjacent modes. Frequency combs were primarily created for frequency metrology but have a growing number of spectroscopic applications including interrogating atomic transitions, environmental sensing, and detecting trace gas impurities [34,43–46]. There are examples of using an OFC, often in conjunction with VIPA spectrometers, to perform human breath analysis in literature that have been highly successful in detecting relevant breath analysis molecules (CO, CO_2, H_2O, CH_4, and NH_3) down to ppb sensitivities and utilising this information to accurately predict SARS-CoV-2 infection [47–52].

In this paper, we further investigate the suitability of using optical frequency combs for human breath analysis. We use baker's yeast (*Saccharomyces cerevisiae*) as an analogue for human breath to test our spectrometer's ability to monitor changing metabolic activity within a living organism. Optical frequency comb spectroscopy is used to measure the concentration of CO_2 produced by the yeast as it metabolises sugars, via techniques demonstrated in Ref. [40] to measure CO_2 and its isotopologues. To improve the sensitivity of these measurements and perform continuous monitoring of concentrations of the two most common isotopologues of CO_2 during these biological processes we use a non-resonant enhancement cell called a Herriott cell. Within this Herriott cell we were able to detect a concentration for $^{12}C^{16}O_2$ as low as 260 ppm (or approximately 2.56×10^{19} molecules within the testing volume of 0.004 m^3) and 175 ppm for $^{13}C^{16}O_2$ (approximately 1.73×10^{19} molecules). By quantifying the amount of CO_2 molecules in this way, we were able to determine the ratio of input-to-output carbon atoms to be 3:1 which matches the ratio expected from fermentation, the dominant metabolic process for baker's yeast.

Biomedical Optics EXPRESS

2. Baker's yeast as a test organism

Baker's yeast (*Saccharomyces cerevisiae*) has historically served as a substitute organism for understanding human cell biology [53–57]. We chose to use this yeast species in our experiment as a substitute for analysing human breath samples because: (a) it produces carbon dioxide (CO_2) in a moist environment similar to human breath, and (b) the amount of CO_2, and the rate at which it is produced, depends on the yeast's metabolism, which we can affect by changing environmental parameters.

S. cerevisiae can metabolise a wide variety of carbon sources although it prefers sugars [58–61]. Here we use both sucrose and glucose, and note that the metabolism of these two sugars is nearly identical since *S. cerevisiae* breaks down polysaccharides, such as sucrose, into glucose molecules via enzymes [62].

Yeast metabolises sugars differently depending on whether they are being used for energy or to create new biomass. In this paper we are only interested in the ways that *S. cerevisiae* metabolises sugar to produce CO_2. Yeast can metabolise glucose into CO_2 by one of two metabolic pathways: respiration, (see Eq. (2)) and fermentation (see Eq. (3)). Note that Eqs. (2) and (3) represent a simplification of metabolic processes [58,63–67].

$$C_6H_{12}O_6 + 6O_2 \longrightarrow 6CO_2 + 6H_2O \tag{2}$$

$$C_6H_{12}O_6 \longrightarrow 2CO_2 + 2C_2H_5OH. \tag{3}$$

S. cerevisiae may perform both respiration and fermentation simultaneously, but only if the available concentration of sugar is high enough. Below a certain sugar concentration (approx. 100-150 mg/L), *S. cerevisiae* will metabolise available nutrients via respiration. If this concentration is surpassed then the yeast will ferment the additional sugar, even under aerobic conditions, leading to a mixed metabolism of both respiration and fermentation, a process referred to as the Crabtree effect [58,68–70]. Given the sugar concentrations in this experiment are much higher than this threshold, we expect our yeast samples to mostly ferment the available sugars.

We can affect the amount and rate of CO_2 production by changing the starting sugar mass and the temperature [71]. For example, changing the initial mass of the glucose in Eq. (3) produces a proportional change in the final amount of CO_2. In addition, there is a temperature dependence to the rate of fermentation and thus CO_2 production [71]. By changing the environmental parameters to affect the metabolic output of *S. cerevisiae*, we created a proof of concept for measuring changing gas concentrations, such as CO_2, in human breath. We also examined the outcomes of feeding *S. cerevisiae* mixed ratios of isotopic glucose, measuring the total concentration of each CO_2 isotopologue. To measure the CO_2 concentration produced by *S. cerevisiae*, we utilise direct frequency comb spectroscopy, which enables accurate concentration measurements as well as the capacity to detect multiple isotopes.

3. Experimental method

There are two components to the experiment: an optical system, and a gas system. The optical apparatus performs direct frequency comb spectroscopy, and the gas apparatus that controls, siphons, and dries gas from the headspace above the *S. cerevisiae*, which is grown under controlled conditions. The optical apparatus has been developed over the course of previous work and used for the precise measurement of hydrogen cyanide, carbon dioxide (both $^{12}CO_2$ and $^{13}CO_2$), and acetylene [39–42].

3.1. Optical apparatus

The frequency comb used to perform direct frequency comb spectroscopy of the sample was a Menlo Systems FC1500 spanning 1500 nm-1700 nm. The repetition rate, f_{rep}, of the comb is

Biomedical Optics EXPRESS

250 MHz, and is locked to a cavity-stablised CW laser (1560 nm NKT Koheras Boostik E15). The carrier-envelope offset frequency, f_0, is locked to 20 MHz via f-$2f$ locking to a cesium-beam clock (Datum CsIII).

Comb light is first split equally into two pathways: the spectroscopy pathway and the rarefaction pathway as shown in Fig. 1. The *spectroscopy pathway* is further divided by a wedged beam splitter (WBS) into a sample and reference path. Reference path light is retro-reflected back towards the WBS without absorption by the molecular sample, as a reference measurement of the comb power at each wavelength. The sample path light is directed into a non-resonant, sealed, multi-pass Herriott cell by way of a periscope. The sample path is retro-reflected to double pass the Herriott cell for a total optical path length of 60 m. Gas is pumped through a closed loop from a Buchner flask containing the yeast through the Herriott cell, before returning to the flask. Both sample and reference paths are equipped with an automated optical shutters to select which path is being observed, and coupled into optical fiber to be directed towards the spectrometer.

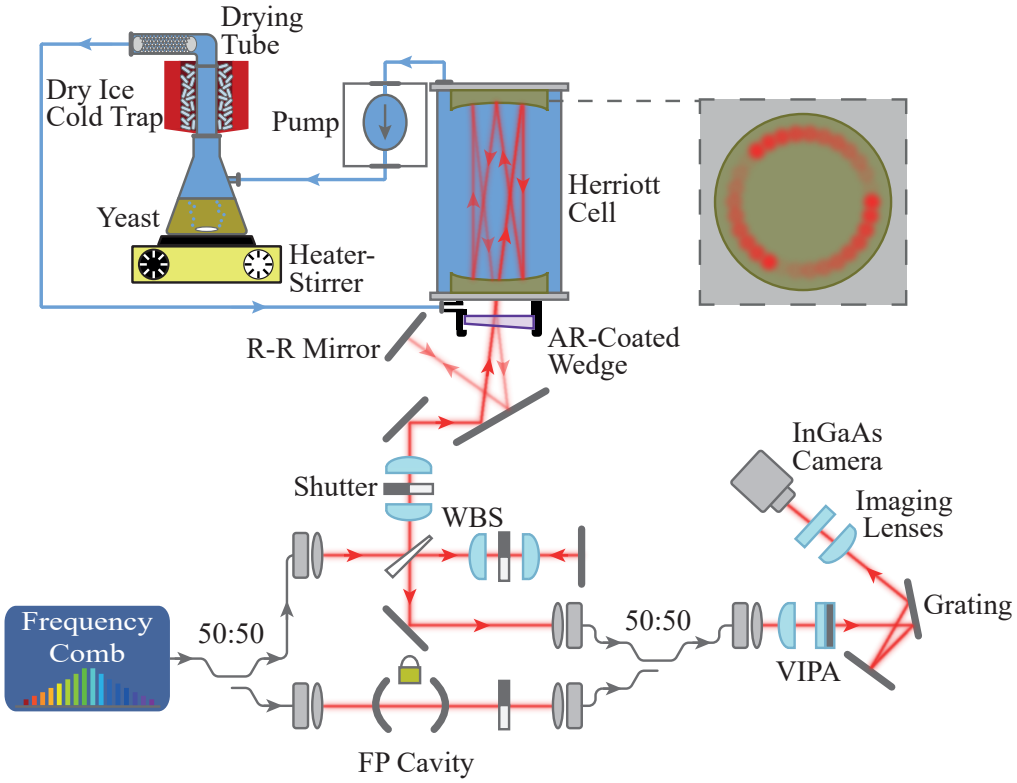

Fig. 1. A simplified diagram of the experiment. FP: Fabry-Perot (cavity); WBS: Wedged beam splitter; RR: Retro-reflection (mirror). Fiber-coupled paths are represented in grey, free-space optical paths are coloured red, with increased transparency indicating the beam has passed through the Herriott cell once already. Gas paths are represented as light blue, with blue areas indicating the presence of gas. The dotted line inset displays a rough diagram of the reflection pattern of the beam on each Herriott cell mirror.

A rarefaction pathway leads into a low-finesse optical cavity with a free-spectral-range of $36\times f_{rep} \approx 9$ GHz. This rarefies the comb frequency spacing so that only every 36th comb mode remains. Our spectrometer is then able to resolve each comb mode individually, allowing calibration of the frequency of each mode [40]. Light from the rarefied comb is coupled into optical fiber and directed towards the spectrometer.

Biomedical Optics EXPRESS

The spectrometer consists of a Virtually-Imaged Phased Array (VIPA) etalon with a finesse of approximately 200 and a free-spectral-range of 50 GHz, followed by an orthogonally-placed diffraction grating with 600 lines/mm [39,40]. A VIPA disperses the comb frequencies vertically and, to prevent frequency overlap, the diffraction grating horizontally disperses comb modes that spatially overlap due to the limited Free Spectral Range (FSR) of the etalon. The grating is double-passed for greater horizontal separation to minimise cross-talk between VIPA stripes [40]. The resulting 2D comb mode array is imaged onto an InGaAs Camera (Xenics XEVA-1.7-320) over an integration time of 1s per shot. The spectrometer camera acquires six images per optical spectrum, including two images for each of the sample, reference and cavity paths: a bright/dark image with the shutters open/closed each with equal integration times. The spectrometer is capable of measuring 25 nm of the optical spectrum at a time. This spectrometer has been shown to produce precise and accurate number density measurements, in particular for CO_2 [40,41]. For further information on the design, precision, and accuracy of this VIPA spectrometer in measuring controlled quantities of hydrogen cyanide, CO_2, and acetylene, see Ref. [39–42].

For trials 1–7, in which we tested *S. cerevisiae* under different environmental conditions, we wished to monitor the strongest $^{12}C^{16}O_2$ transitions. To achieve this, the spectrometer grating was adjusted to capture the 30012 ⟵ 00001 ro-vibrational transitions of $^{12}C^{16}O_2$ located between wavenumbers 6293 cm^{-1} and 6395 cm^{-1} (1563.72 nm - 1589.07 nm) as given by the HITRAN database [72]. For trials 8–10, in which we desired to measure transitions for $^{12}C^{16}O_2$ and $^{13}C^{16}O_2$ simultaneously, the grating was moved to observe between 6178 cm^{-1} and 6273 cm^{-1} (1594.12 nm - 1618.65 nm) to measure the 30013 ⟵ 00001 transitions and 30012 ⟵ 00001 transitions of each isotopologue, respectively as given by the HITRAN database [72].

3.2. Yeast apparatus

Dry yeast was placed into a 500 mL Buchner flask, along with distilled water and either sucrose or glucose. The flask was placed on a heater-stirrer which was capable of both temperature control and spinning a magnetic stirrer to gently disturb the mixture to release any trapped CO_2. We maintained a closed, low airflow gas loop by way of an air pump moving the gas from the headspace above the baker's yeast into the Herriott cell and back out again. Moisture in the gas mixture was reduced by passing it through a cold trap and drying column in series.

In Table 1 we summarise the different environmental conditions for the 10 different trials we performed. For trials 1–7, we measured the Yeast's metabolic output under different environmental conditions and monitored changes in the CO_2 concentration profile between trials. To modify the environment we varied the temperature, as well as the amount and type of nutrients available to the yeast using different proportions of glucose or sucrose. For trials 8–10, we measured the concentration profile of two different isotopologues of CO_2 simultaneously. This was achieved by altering the ratio of store-bought glucose, naturally abundant in carbon-12 and carbon-13, and D-glucose-$^{13}C_6$ ($C_6^{13}H_{12}O_6$). For each trial, a single spectrum was recorded every minute, beginning immediately after the addition of the sugar, and lasting a typical run time of approximately four hours. This was sufficiently long to reliably observe most of the dynamics of the yeast's metabolism, though in some cases was not quite long enough to stop completely, such as in trials 3, 8, 9, and 10.

Biomedical Optics EXPRESS

Table 1. Feed-stock and environmental parameters for each trial.

Trial	Time (min)	Temp. (°C)	Yeast (g)	Sucrose (g)	Glucose (Nat.Abd.) (g)	Glucose (C-13) (g)
1	360	30 ± 1	3.07 ± 0.01	2.03 ± 0.01	-	-
2	360	30 ± 1	3.05 ± 0.01	4.13 ± 0.01	-	-
3	274	30 ± 1	6.057 ± 0.001	2.037 ± 0.001	-	-
4	420	30 ± 1	6.032 ± 0.001	4.086 ± 0.001	-	-
5	420	30 ± 1	3.000 ± 0.001	-	2.020 ± 0.001	-
6	356	35 ± 1	3.021 ± 0.001	-	2.063 ± 0.001	-
7	372	22 ± 2	3.004 ± 0.001	-	2.015 ± 0.001	-
8	254	30 ± 1	6.002 ± 0.001	-	3.500 ± 0.001	0.503 ± 0.001
9	250	30 ± 1	6.001 ± 0.001	-	3.001 ± 0.001	1.003 ± 0.001
10	238	30 ± 1	6.002 ± 0.001	-	2.501 ± 0.001	1.477 ± 0.001

4. Image analysis

To extract the CO_2 concentration, the spectrometer images must first be converted into molecular transmission spectra. Further detail on the following, including the effect of the number of pixels upon detection ability, can be found in Refs. [40,42]. First, the dark images are subtracted from their corresponding bright images to remove camera background effects. From this we are left with images of vertical bright stripes for both the sample and reference path images as the spectrometer cannot resolve individual comb modes without the rarefaction cavity, see Ref. [39,40]. To minimise cross-talk between adjacent VIPA stripes to below the measurement noise and maximise the signal-to-noise ratio, we apply a series of Gaussian matched filters to the images [40]. The filters are based on the horizontal cross-section of each stripe from the reference image, which is approximately a Gaussian profile, and are applied to the signal and cavity images. This filter applies a low weighting in-between the stripes where the crosstalk is greatest, and maximises the weighting in the centre of the stripes where crosstalk is minimal and the signal is strongest. The result is a single representative brightness point for each row of each stripe. We then divide the filtered sample signal by the filtered reference signal which is unwrapped into a ro-vibrational transmission spectrum.

A relative frequency axis for the molecular transmission spectrum is derived using the resolved modes from the cavity rarefied image as well as the cavity FSR and known comb parameters (f_{rep} and f_0). The absolute frequency is obtained by shifting this relative axis using spectral positions from the HIgh-resolution TRANsmission (HITRAN) molecular absorption database [72].

5. Spectral fitting

To extract the CO_2 concentration we fit each ro-vibrational transition with a model transmission spectrum based on a Voigt line profile. Each Voigt profile is scaled by $\tau_i = S_{\eta\eta'}(T)\, u\, L$, the optical depth of the i-th ro-vibrational transition with lower level η and upper level η'. The concentration, u, and temperature, T, are left as free variables, while the interaction length, L, is fixed based on a measurement of the Herriott cell filled with 100% CO_2 (natural isotopic abundances) to calibrate the optical path length. The overall transmission spectrum is then the summation of these individual Voigts, $V(\nu - \nu_i, T, P)$, as given by:

$$\mathcal{T}(\nu, T, P) = \exp\left[-\sum_i \tau_i V(\nu - \nu_i, T, P)\right], \tag{4}$$

Biomedical Optics EXPRESS

where ν is the wavenumber, ν_i is the line centre, T is the temperature, and P is the total pressure of the gas as described in Refs. [40,72]. We include several fixed parameters from the HITRAN database, including the line strength $S_{\eta\eta'}(T_{ref})$ at a reference temperature $T_{ref} = 296$K, lower state energy of the transition E_η, the line centre frequency $\nu_{\eta\eta'}$, and the pressure shift of the line centre.

The temperature-dependent line strength is given by [72]:

$$S_{\eta\eta'}(T) = S_{\eta\eta'}(T_{ref})\frac{Q(T_{ref})}{Q(T)}\frac{e^{\frac{c_2 E_\eta}{T}}}{e^{\frac{c_2 E_\eta}{T_{ref}}}}\frac{1-e^{\frac{c_2\nu_{\eta\eta'}}{T}}}{1-e^{\frac{c_2\nu_{\eta\eta'}}{T_{ref}}}} \tag{5}$$

where $c_2 = hc/k_B$, h is Planck's constant, c is the speed of light, and k_B is Boltzmann's constant. The $Q(T)$ terms are the complex molecular total internal partition function of CO_2 and are temperature-dependent. This function is computationally intensive and so a polynomial approximation to the partition function is used instead [73].

The Lorentzian and Gaussian components of the Voigt lineshape are a combination of molecular properties and spectrometer broadening. Lorentzian collisional broadening coefficients are taken from the HITRAN database, whilst the temperature-dependent Doppler Gaussian contribution is calculated to be approximately $0.0049 \pm 0.00005\,\mathrm{cm}^{-1}$ ($1/e$ half-width) across all trials and for both isotopologues. Systematic spectrometer line broadening of the spectra is also included, with the Lorentzian and Gaussian spectrometer contributions being $0.01 \pm 0.001\,\mathrm{cm}^{-1}$ and $0.012 \pm 0.001\,\mathrm{cm}^{-1}$ respectively, as measured previously [40]. The Gaussian contributions from the Doppler and spectrometer broadening mechanisms are combined via a quadrature sum.

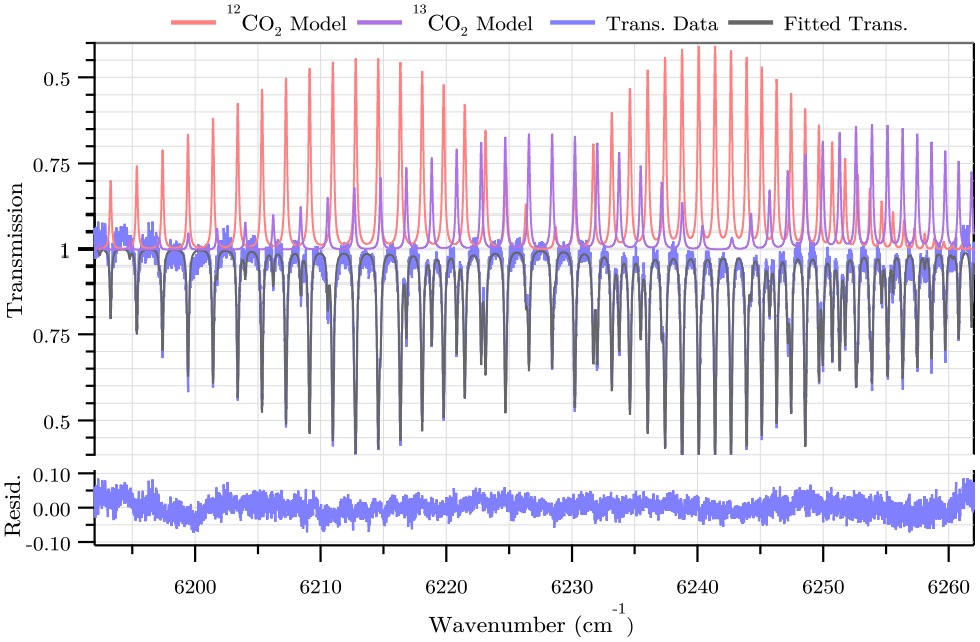

Fig. 2. Top: Ideal model based on HITRAN parameters of the transitions $^{12}C^{16}O_2$ (30013 ⟵ 00001), in red, and $^{13}C^{16}O_2$ (30012 ⟵ 00001), in purple. Middle: Fitted transmission data taken from the final minute of trial 10 showing absorption of the comb light from the gas in the Herriott cell. The model (blue) is fitted closely to the measurement data (grey). Bottom: The residuals between the raw data and the fit, which show confirms the high quality of the fit.

Biomedical Optics EXPRESS

There is an additional third-order polynomial included in the model to account for broad background variations, and is obtained from fitting to the first captured spectra of each trial when only atmospheric CO_2 is present. Additionally included in the background fitting are etalons of varying amplitude and frequency that change between trials which are present within the optical setup. The presence of these background transmission etalons necessitated manual selection of initial conditions for each trial, disallowing true real-time monitoring. However, in the absence of these etalons such monitoring is possible [40].

To extract concentration using this spectroscopic model we performed a least-squares fit of our model to each spectrum, leaving temperature, T, number density, u, and our background parameters as free variables. An example of a single-shot spectrum can be seen in Fig. 2. This spectrum was acquired when all available sugars had been consumed and shows the deepest molecular absorption spectrum captured at the end of trial 10. The residuals in Fig. 2 are mainly attributed to a small-scale high-frequency etalon that was unable to be successfully fitted in the background fitting stage. The residuals show that we can expect our optical setup to detect absorption features around 5 % in transmission in a single measurement. This sensitivity has been shown to improve with additional averaging [40].

6. Results

We used our setup to perform 10 trials, changing the environmental parameters that affect *S. cerevisiae*'s metabolism and production of CO_2. Each trial took place over several hours and a single spectra was captured every minute. The spectra were fitted to extract isotopic concentrations of CO_2 and monitor their changes over time. The different trial parameters are recorded in Table 1, with the extracted CO_2 concentrations over time presented in Figs. 3–5. Tables 2, 3, 4, 5, 6, and 7 summarise different aspects of the measured CO_2 evolution in each trial. Tables 2, and 5–7 summarise the CO_2 concentration after metabolism had completed, which was calculated by averaging the final 50 concentration measurements in a run, which form the plateau of the CO_2 profiles. Tables 3 and 4 summarise the production rate of CO_2 which are calculated by fitting the CO_2 concentration over a time period where the rate of change is approximately linear, i.e. after the initial exponential increase and before the plateau in concentration.

Table 2. Comparing ratios of starting sugar amount to ratios of CO_2 concentration.

Trial	Starting Sugar Ratio	CO_2 Conc. Ratio
2/1	2.03 ± 0.01	1.83 ± 0.02
4/3	2.006 ± 0.001	1.77 ± 0.03

Table 3. Comparing ratio of starting yeast amount to ratios of CO_2 production rate.

Trial	Starting Yeast Ratio	CO_2 Rate Ratio
4/2	1.97 ± 0.006	1.44 ± 0.04
3/1	1.97 ± 0.006	2.53 ± 0.09

In trials 1–7, we monitored how the CO_2 concentration changes as the metabolism of *S. cerevisiae* shifts in response to changes to its environment. The CO_2 profiles shown in Fig. 3 and 4 closely match the typical growth profile for *S. cerevisiae* [74–80]. These trials involved varying the amount of yeast, amount of sugar, as well as temperature, to measure how the CO_2 profile evolves differently - changing both the amount of CO_2 produced, as well as the rate of production.

For trials 1–4, we altered the starting amounts of yeast and sugar. The evolution of the measured CO_2 concentration are presented in Fig. 3. From Eq. (2), we expect the ratio of CO_2 concentration

Biomedical Optics EXPRESS

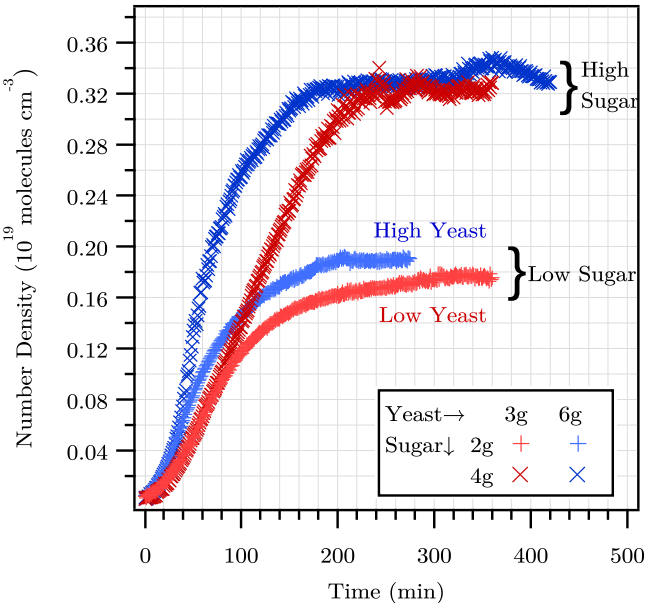

Fig. 3. The concentration of CO_2 within the Herriott cell during trials 1–4. A spectrum was recorded at every minute.

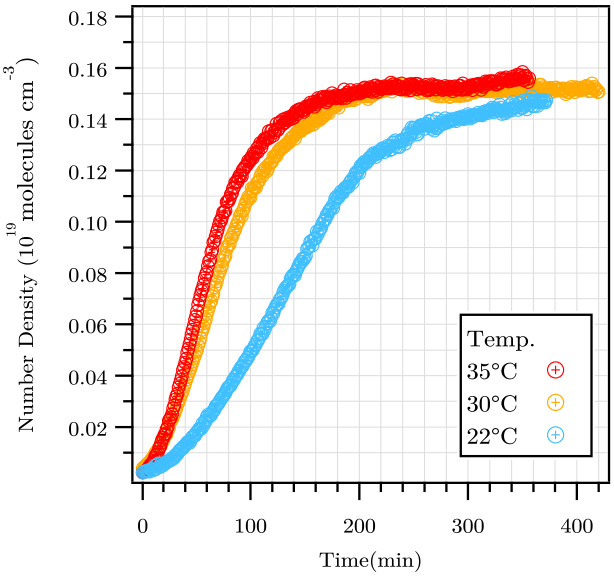

Fig. 4. The concentration of CO_2 within the Herriott cell during trials 5–7. A spectrum was recorded at every minute.

Table 4. The linear rate of change in CO_2 concentration with temperature.

Trial	Temp. (°C)	Rate ($\times 10^{19}$ molecules.cm^{-3}.min^{-1})
5	30	13.9 ± 0.2
6	35	17.5 ± 0.2
7	22	7.45 ± 0.05

Biomedical Optics EXPRESS

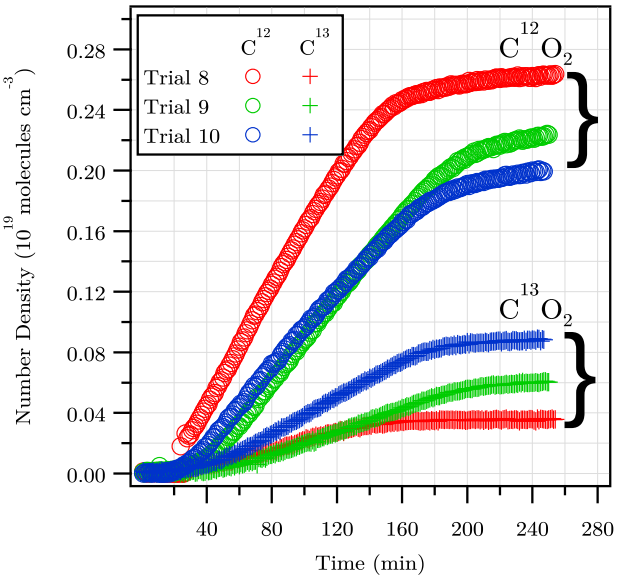

Fig. 5. The concentration of $^{12}C^{16}O_2$ and $^{13}C^{16}O_2$ within the Herriott cell. A spectrum was recorded at every minute. The fitting algorithm failed to fit spectra from the first approx. 30 minutes of trial 8, hence the discontinuity in the plot.

Table 5. Isotope Ratios.

Trial	Input Mass Ratio (β_{in})	Output CO_2 Ratio (β_{out})	Prop. of ^{13}C emitted (α)
8	0.1563 ± 0.0003	0.136 ± 0.002	0.89 ± 0.01
9	0.3490 ± 0.0005	0.27 ± 0.01	0.82 ± 0.03
10	0.6082 ± 0.0007	0.45 ± 0.01	0.82 ± 0.01

Table 6. The number of carbon-12 atoms ($\times 10^{22}$ atoms) input into the testing volume as sucrose/glucose, and output as CO_2. Ratio of carbon atoms input to output.

Trial	$^{12}C_{Sugar}$ In	$^{12}CO_2$ Out	$^{12}C_{Out}/^{12}C_{In}$[%]
1	4.29 ± 0.02	1.51 ± 0.11	35.3 ± 2.9
2	8.72 ± 0.02	2.77 ± 0.22	31.8 ± 2.6
3	4.300 ± 0.002	1.62 ± 0.12	37.8 ± 2.9
4	8.626 ± 0.002	2.88 ± 0.24	33.4 ± 2.8
5	4.051 ± 0.002	1.30 ± 0.10	32.1 ± 2.4
6	4.138 ± 0.002	1.33 ± 0.10	32.1 ± 2.5
7	4.041 ± 0.002	1.25 ± 0.10	30.8 ± 2.5
8	7.020 ± 0.002	2.24 ± 0.17	32.0 ± 2.4
9	6.019 ± 0.002	1.87 ± 0.17	31.1 ± 2.8
10	5.017 ± 0.002	1.68 ± 0.14	33.5 ± 2.9

Biomedical Optics EXPRESS

Table 7. The number of carbon-13 atoms ($\times 10^{22}$ atoms) input into the testing volume as sucrose/glucose, and output as CO_2. Ratio of carbon atoms input to output.

Trial	$^{13}C_{Sugar}$ In	$^{13}C_{CO_2}$ Out	$^{13}C_{Out}/^{13}C_{In}$[%]
8	0.976 ± 0.002	0.31 ± 0.02	31.3 ± 2.6
9	1.947 ± 0.002	0.51 ± 0.05	25.9 ± 2.4
10	2.868 ± 0.002	0.75 ± 0.06	26.1 ± 2.1

to double with a doubling of the input sugar. Figure 3 shows this rough proportionality, with trials 1 and 2 doubling sugar (a constant 3 grams of yeast) having a final CO_2 concentration ratio of 1.83 ± 0.02, and for trials 3 and 4 (6 g of yeast) a ratio of 1.77 ± 0.03. These results are summarised in Table 2. This slight discrepancy may be due to some of the additional nutrients being invested in increased yeast budding rather than being metabolised.

Conversely, when the amount of yeast is doubled and the amount of sugar held constant, we expect an increase in the rate of CO_2 production. Table 3 summarises input yeast amounts and the observed rate increases. As expected, when the starting yeast mass was doubled there was an increase in the rate of CO_2 production by a factor of 1.44 for trials 2 to 4, and approximately 2.53 from trials 1 to 3. The trials with a higher sugar starting mass (≈4 g) had a much larger rate increase in CO_2 production when the initial yeast mass was doubled, compared to the trials in which the sugar mass was lower (≈2 g), suggesting that the two yeast growth factors (initial sugar and yeast masses) compound together to produce a much higher production rate.

In trials 5–7, we kept masses of the yeast and glucose constant, and monitored the effect of changing the temperature of the system. Figure 4 demonstrates that increasing the temperature results in an increased CO_2 production rate which is summarised in Table 4. This is expected due to the faster metabolic rate of the yeast induced by a higher temperature. The growth rate increase when the temperature is increased from 22 °C to 30 °C is much larger than that between 30 °C and 35 °C. This is because the optimum temperature range for growth of most yeast species is between 20 °C to 30 °C, with yeast beginning to perish faster than it can reproduce above approximately 40 °C [71,81–83]. The optimum temperature to maximise yeast growth rate depends on a number of factors including yeast species, pH, water activity, and the presence of antimicrobial substances such as the ethanol produced by the yeast [71].

In trials 8–10 *S. cerevisiae* was fed several ratios of radioisotope-labelled glucose ($^{13}C_6H_{12}O_6$) and non-labelled glucose ($^{12}C_6H_{12}O_6$). Each trial incrementally increased the amount of $^{13}C_6H_{12}O_6$ by 0.5 g and correspondingly decreased the amount of $^{12}C_6H_{12}O_6$ by 0.5 g, as summarised in Table 1. Our spectrometer is able to measure the spectra of multiple isotopologues of CO_2 simultaneously, thus we can monitor the concentration of these isotopologues as they were produced by the yeast. An example spectra from trial 10 is shown in Fig. 2 displaying absorption features from both $^{13}C_6H_{12}O_6$ and $^{12}C_6H_{12}O_6$. The measured time dependence of the CO_2 isotopologue concentrations for all three of these trials are displayed in Fig. 5. The number density of both isotopologues across all trials qualitatively match the typical CO_2 profile of baker's yeast provided an initial amount of sugars to consume [74–80]. As expected, the number density of $^{13}C^{16}O_2$ increases proportionally to the amount of labelled glucose added. However, the concentration of $^{12}C^{16}O_2$ does not decrease by the observed increase in $^{13}C^{16}O_2$.

To better understand how the different isotopologues are metabolised, we calculate the carbon-13/12 ratio of the input glucose to the output CO_2 which is summarised in Table 5. We observe a difference between the input and output carbon-13/12 ratios due to the incorporation of carbon from the sugars into the biomass of the yeast and subsequent exhalation of carbon that was once part of the yeast biomass [67]. This biomass is the energy storage of the yeast, glycogen, which are comprised of long chains of glucose which are consumed if a yeast cell is unable to access external nutrients [84]. This glycogen glucose is metabolised via the same pathways. We denote

Biomedical Optics EXPRESS

the efficiency of the metabolism of ^{13}C from glucose to CO_2 as α and so can be represented as:

$$^{13}\mathrm{C}_{\mathrm{out}} = \frac{1}{3}\,\alpha\,{}^{13}\mathrm{C}_{\mathrm{in}}. \tag{6}$$

Correspondingly the proportion of ^{13}C which becomes embedded in the biomass is $1-\alpha$, where we hypothesise that each ^{13}C incorporated results in a molecule of $^{12}CO_2$ emitted, such that:

$$^{12}\mathrm{C}_{\mathrm{out}} = \frac{1}{3}\left({}^{12}\mathrm{C}_{\mathrm{in}} + (1-\alpha)\,{}^{13}\mathrm{C}_{\mathrm{in}}\right). \tag{7}$$

The $1/3$ prefactor in Eqs. (6) and (7) is because yeast metabolism is predominantly a fermentative process as described by Eq. (3), in which $1/3$ of carbon atoms introduced become CO_2. Here we have assumed that the initial biomass of the yeast is entirely ^{12}C.

Combining Eqs. (6) and (7) gives an expression for the ratio of carbon-13/12 expelled from the yeast, as a function of input carbon-13/12 ratio as:

$$\beta_{\mathrm{out}} = \frac{\alpha\,\beta_{\mathrm{in}}}{1+(1-\alpha)\beta_{\mathrm{in}}} \tag{8}$$

where $\beta_{\mathrm{in}} = {}^{13}\mathrm{C}_{\mathrm{in}}/{}^{12}\mathrm{C}_{\mathrm{in}}$ and $\beta_{\mathrm{out}} = {}^{13}\mathrm{C}_{\mathrm{out}}/{}^{12}\mathrm{C}_{\mathrm{out}}$. This gives the proportion of ^{13}C which is metabolised and ejected as $^{13}CO_2$, α, as:

$$\alpha = \frac{\beta_{\mathrm{out}}}{1+\beta_{\mathrm{out}}}\,\frac{1+\beta_{\mathrm{in}}}{\beta_{\mathrm{in}}}. \tag{9}$$

Table 5 summarises the input and output carbon-13/12 ratios and calculated α for each of the relevant trials. The value of α is observed to be consistent across all trials being roughly 0.84. As per Eq. (6), the percentage of input ^{13}C metabolised into CO_2 was $0.84\times 1/3 \approx 28$ %, whilst the remaining $0.16\times 1/3 \approx 5$ % is incorporated into the yeast as biomass. We expect this would be true for both isotopologues, that is ≈28 % of the input glucose is converted into CO_2 while ≈5 % is incorporated into biomass. Over time, if *S. cerevisiae* had been fed continuously on a fixed ratio of carbon-12/13 glucose, we would expect the exhaled CO_2 isotopologues to approach the input ratio. This may explain why the CO_2 number density for both isotopologues doesn't appear to have reached equilibrium by the end of trials 8–10.

To analyse the limitations of our concentration measurements, we use trials 8–10 as these were the trials that contained both ^{12}C and ^{13}C, and from these trials we considered only the final 50 measurements as the concentration of CO_2 in the system at that point was relatively stable. While the last 50 measurements were near equilibrium, there are still slow changes in CO_2 concentrations. This effect was subtracted out via a linear fit to the final 50 points of the concentration data, with the standard deviation of the resulting data used to estimate the concentration noise. If we consider the standard deviation to be the minimum measurable change in the concentration, then on average our spectrometer is capable of a minimum observed change in $^{12}C^{16}O_2$ of approximately 6.5×10^{15} molecules cm^{-3}, or 260 ppm with respect to air at Standard Temperature and Pressure (STP). Likewise for $^{13}C^{16}O_2$, we find our instrument can detect a minimum concentration of 4.4×10^{15} molecules cm^{-3}, or approximately 175 ppm. These values are supported by the first observable increase in CO_2 concentration, within the first few minutes, being on average approximately 5×10^{15} molecules cm^{-3} across all three trials. A potential reason for the ^{13}C uncertainty being lower than for ^{12}C is the quantity of ^{13}C glucose was smaller leading to smaller drifts towards the end of each trial. The average relative uncertainty (based on the standard deviation and average CO_2 across the last 50 points) across the last three trials for $^{12}C^{16}O_2$ was around 0.29 % with the highest value of 0.36 % for trial 9, and for $^{13}C^{16}O_2$ an average of 0.81% with the largest relative error being 1.15 % for trial 8. Noting the volume of the

Biomedical Optics EXPRESS

Herriott Cell is approximately 0.004 m^3, we can infer the smallest detectable number of $^{12}C^{16}O_2$ molecules within our Herriott cell to be 2.57×10^{19} molecules. Likewise for $^{13}C^{16}O_2$ we can quantitatively say the smallest number of molecules detectable by our spectrometer is 1.73×10^{19}.

As the experiment is a closed system with known volume, we can investigate the mass balance - a comparison of the number of carbon atoms introduced as glucose to the number which become CO_2 - of carbon atoms within the system. Since *S. cerevisiae* is predominantly fermentative, we would expect that the ratio of input carbon (as sugar) to output carbon (as CO_2) to be $1/3$, according to Eq. (3). The results are shown in Tables 6 and 7, which summarise the number of carbon atoms introduced to the yeast system as glucose/sucrose, and the number of carbon atoms out. The carbon atoms out were calculated from the final 50-data point average CO_2 concentration at the end of each trial and the volume of the system which was measured to be 0.0086 ± 0.0006 m^3. We see close agreement to the expected carbon in-out ratio of $1/3$ with an average over all trials of 33 ± 3 %. We note the amount of atmospheric CO_2, approximately 420 ppm, is negligible compared to the amount of CO_2 in the Herriott cell at the end of the trials, and should not perturb this measurement.

We can connect these input/output ratios to our earlier results, where we compared the quantity of CO_2 produced under different conditions. For example, trials 1 and 3 (which contained ≈ 2 g of sugar) have a $^{12}C_{Out}/^{12}C_{In}$ ratio that is ≈ 4 % higher than their counterpart trials 2 and 4 which started with double the initial nutrient amounts (≈ 4 g of sugar). This discrepancy is noted in Table 2 where a doubling of the input sugar lead to an increase in CO_2 production, but less than a factor of two increase. Examining the input/output carbon ratios indicates that this discrepancy from a factor of two increase may be due to trials 1 and 3 having an increased conversion efficiency above 33 %. Likewise, we noted that the production of $^{13}CO_2$ indicated that the isotopically labelled sugar was being incorporated into biomass, as summarised in Table 5, which is also seen in Table 7 as an output ratio significantly below 33 %. Thus, calculating the percentage of carbon that is emitted as CO_2 has helped explain why our earlier results did not meet expectations.

7. Discussion

A major challenge for molecular spectroscopy in the near-infrared (near-IR) region being investigated here is the presence of water vapour that can deteriorate optical systems and contaminate the molecular spectral signature of interest. Using *S. cerevisiae* as a substitute for human breath enabled us to test methods of removing water vapour from the gas sample being probed. There are H_2O transitions present in the measurement wavelength ranges with line strengths approximately 100 times weaker than those of CO_2. Consequently, since the transmission residuals have a noise of approximately 1%, the concentration of H_2O would need to be on the order of 10^{18} molecules per centimetre cubed to be observed in our spectra.

We have been able to demonstrate several ways in which our spectrometer could be used for human breath analysis. Most notable is the capability of our spectrometer to distinguish isotopologues of CO_2 produced by the yeast in response to the addition of isotopically-labelled glucose. This is analogous to a test that could be performed on a human being. Several such medical tests are in development to measure exhaled CO_2 to monitor patient health such as the field of capnography, and via the ingestion of isotopically-labelled substances diagnose infectious diseases and monitor the metabolic health of a patient [85–88]. Our spectrometer's minimum measureable concentrations for $^{12}C^{16}O_2$ and $^{13}C^{16}O_2$ were 260 ppm and 175 ppm respectively. In comparison to human breath which has a CO_2 concentration in the range of 35,000 ppm - 50,000 ppm, these measurements correspond to a change of CO_2 concentration in a persons breath of approximately 0.5-0.7 % [89]. Taking this one step further, based on this concentration of CO_2 and assuming a natural abundance of ^{13}C in a person's breath, a person may exhale up to approximately 400-500 ppm $^{13}C^{16}O_2$ which is theoretically detectable by our instrument.

Biomedical Optics EXPRESS

By enhancing the sensitivity of our instrument further, we may improve its diagnostic and monitoring capabilities. A significant demonstration of this device for human breath testing would be to match or outperform the performance of the existing ^{13}C-Urea breath test for diagnosing the presence of *H. pylori*, a type of gut bacteria which can cause stomach ulcers [90]. Most tests will measure the δ^{13}C of a patient before and after they have ingested a tablet of ^{13}C-labelled urea: the ratio of ^{13}C to ^{12}C in a sample, divided by the same ratio of a reference material. A difference greater than $2-5\times10^{-3}$ generally indicates the test is positive [91]. If we consider that the isotopic abundance of CO_2 in a person's breath is the same as the surrounding air, then a positive test would indicate an increase from approximately 385 ppm to 392 ppm. Our minimum detectable concentration for ^{13}C was 175 ppm, hence improvement is required.

To improve the performance of our instrument to this level, changes to the spectrometer are required to improve its isotopic sensitivity. The transitions examined in this paper in the near-IR are overtones of much stronger, fundamental transitions in the mid-infrared (mid-IR) [72]. Utilising a mid-IR comb would therefore offer a significant sensitivity advantage due to an increased absorption signal, enabling the detection of much smaller concentrations of biomarkers as found in human breath [34,92]. Additional sensitivity gains could be achieved by increasing the effective optical path length of the sample cell, as this would provide further opportunities for interactions between the probing light and the molecules [93]. This can be done by acquiring a cell with a longer effective optical path length, either a resonant optical cavity or a longer multi-pass cell [94]. While these techniques will improve signal strength, the noise can be reduced through a combination of: increasing the optical power of the probing light, utilising low-loss mirror coatings to maximise throughput of the multi-pass cell, and a reduction in the spectrometer detection noise.

8. Conclusion

We presented an optical spectrometer that shows potential use for medical diagnosis based on breath analysis. A frequency comb and VIPA spectrometer were used to measure CO_2 produced by *Saccharomyces cerevisiae* under different environmental conditions as an analogue for human breath. The incorporation of a Herriott multi-pass cell gave our system the sensitivity to detect CO_2 at comparable concentrations to human breath. Our spectrometer is able to observe the changing metabolism of a living organism through monitoring the concentration of CO_2 it produces. We observed the expected changes produced by varying the temperature, type and amount of sugar and quantity of yeast. By quantifying the number of CO_2 molecules and comparing the ratio of carbon input/output we were also able to determine the expected metabolic process, fermentation, that the yeast was undergoing. Furthermore, we are able to distinguish between and measure different isotopologues simultaneously, in our case $^{12}C^{16}O_2$ (to 260 ppm) and $^{13}C^{16}O_2$ (to 175 ppm), which we tested using isotopically-labelled sugars. We were able to verify our results by examining the carbon balance of the measurements via the proportion of carbon which became CO_2 compared to the proportion which was incorporated into the yeast biomass.

Funding. Asian Office of Aerospace Research and Development (AOARD) (FA2386-20-1-4047); Australian Research Council (ARC) Centre of Excellence in Optical Microcombs for Breakthrough Science (COMBS) (CE230100006).

Acknowledgments. This work was performed in part at the Optofab node of the Australian National Fabrication Facility utilising Commonwealth and SA State Government funding. In particular, the authors would like to thank Evan Johnson for his assistance in fabricating crucial equipment utilised in these experiments. We acknowledge support from the U.S. AFOSR AOARD FA2386-20-1-4047. This research was conducted by the Australian Research Council Centre of Excellence in Optical Microcombs for Breakthrough Science (project number CE230100006) and funded by the Australian Government.

Disclosures. The authors declare no conflicts of interest.

Biomedical Optics EXPRESS

Data availability. Data and code underlying the results presented in this paper are available from the corresponding author upon reasonable request.

References

1. K.-H. Kim, S. A. Jahan, and E. Kabir, "A review of breath analysis for diagnosis of human health," Trends Anal. Chem. **33**, 1–8 (2012).
2. B. Henderson, A. Khodabakhsh, M. Metsälä, *et al.*, "Laser spectroscopy for breath analysis: towards clinical implementation," Appl. Phys. B **124**(8), 161 (2018).
3. F. D. Francesco, R. Fuoco, M. Trivella, *et al.*, "Breath analysis: trends in techniques and clinical applications," Microchem. J. **79**(1-2), 405–410 (2005).
4. C. Wang and P. Sahay, "Breath analysis using laser spectroscopic techniques: Breath biomarkers, spectral fingerprints, and detection limits," Sensors **9**(10), 8230–8262 (2009).
5. W. Miekisch, J. K. Schubert, and G. F. E. Noeldge-Schomburg, "Diagnostic potential of breath analysis-focus on volatile organic compounds," Clin. Chim. Acta **347**(1-2), 25–39 (2004).
6. T. A. Popoy, "Human exhaled breath analysis," Ann. Allergy, Asthma, Immunol. **106**(6), 451–456 (2011).
7. A. Jordan, S. Haidacher, G. Hanel, *et al.*, "An online ultra-high sensitivity proton-transfer-reaction mass-spectrometer combined with switchable reagent ion capability," Int. J. Mass Spectrom. **286**(1), 32–38 (2009).
8. M. Alonso and J. M. Sanchez, "Analytical challenges in breath analysis and its application to exposure monitoring," Trends Anal. Chem. **44**, 78–89 (2013).
9. T. Bruderer, T. Gaisl, M. T. Gaugg, *et al.*, "On-line analysis of exhaled breath," Chem. Rev. **119**(19), 10803–10828 (2019).
10. L. Pauling, A. B. Robinson, R. Teranishi, *et al.*, "Quantitative analysis of urine vapor and breath by gas-liquid partition chromatography," Proc. Nat. Acad. Sci. U. S. A. **68**(10), 2374–2376 (1971).
11. R. Teranishi, T. R. Mon, A. B. Robinson, *et al.*, "Gas chromatography of volatiles from breath and urine," Anal. Chem. **44**(1), 18–20 (1972).
12. A. Peralbo-Molina, M. Calderón-Santiago, F. Priego-Capote, *et al.*, "Development of a method for metabolomic analysis of human exhaled breath condensate by gas chromatography-mass spectrometry in high resolution mode," Anal. Chim. Acta **887**, 118–126 (2015).
13. C. Deng, J. Zhang, X. Yu, *et al.*, "Determination of acetone in human breath by gas chromatography-mass spectrometry and solid-phase microextraction with on-fiber derivatization," J. Chromatogr. B: Anal. Technol. Biomed. Life Sci. **810**(2), 269–275 (2004).
14. M. G. Wallace, J. D. Pleil, K. D. Oliver, *et al.*, "Non-targeted gc/ms analysis of exhaled breath samples: Exploring human biomarkers of exogenous exposure and endogenous response from professional firefighting activity," J. Toxicol. Environ. Health, Part A **82**(4), 244–260 (2019).
15. R. Su, T. Yang, X. Zhang, *et al.*, "Mass spectrometry for breath analysis," Trends Anal. Chem. **158**, 116823 (2023).
16. B. Buszewski, M. Kesy, T. Ligor, *et al.*, "Human exhaled air analytics: biomarkers of diseases," Biomed. Chromatogr. **21**(6), 553–566 (2007).
17. C. Grote and J. Pawliszyn, "Solid-phase microextraction for the analysis of human breath," Anal. Chem. **69**(4), 587–596 (1997).
18. H. Lord, Y. Yu, A. Segal, *et al.*, "Breath analysis and monitoring by membrane extraction with sorbent interface," Anal. Chem. **74**(21), 5650–5657 (2002).
19. A. Hansel, A. Jordan, R. Holzinger, *et al.*, "Proton transfer reaction mass spectrometry: on-line trace gas analysis at the ppb level," Int. J. Mass Spectrom. Ion Processes **149-150**, 609–619 (1995).
20. W. Lindinger, A. Hansel, and A. Jordan, "On-line monitoring of volatile organic compounds at pptv levels by means of proton-transfer-reaction mass spectrometry (ptr-ms) medical applications, food control and environmental research," Int. J. Mass Spectrom. Ion Processes **173**(3), 191–241 (1998).
21. P. Trefz, M. Schmidt, P. Oertel, *et al.*, "Continuous real time breath gas monitoring in the clinical environment by proton-transfer-reaction-time-of-flight-mass spectrometry," Anal. Chem. **85**(21), 10321–10329 (2013).
22. R. Black, P. Monks, and A. Ellis, "Proton-transfer reaction mass spectrometry," Chem. Rev. **109**(3), 861–896 (2009).
23. R. F. del Rio, M. E. O'Hara, P. Pemberton, *et al.*, "Elimination characteristics of post-operative isoflurane levels in alveolar exhaled breath via ptr-ms analysis," J. Breath Res. **10**(4), 046006 (2016).
24. P. Sulzer, A. Edtbauer, E. Hartungen, *et al.*, "From conventional proton-transfer-reaction mass spectrometry (PTR-MS) to universal trace gas analysis," Int. J. Mass Spectrom. **321-322**, 66–70 (2012).
25. D. Smith and P. Spanel, "Direct, rapid quantitative analyses of bvocs using sift-ms and ptr-ms obviating sample collection," Trends Anal. Chem. **30**(7), 945–959 (2011).
26. P. Spanel and D. Smith, "Selected ion flow tube mass spectrometry for on-line trace gas analysis in biology and medicine," European Journal of Mass Spectrometry **13**(1), 77–82 (2007).
27. D. Smith and P. Spanel, "Status of selected ion flow tube mass spectrometry; accomplishments and 3 challenges in breath analysis and other areas," Bioanalysis **8**(11), 1183–1201 (2016).
28. P. Spanel and D. Smith, "Progress in sift-ms: Breath analysis and other applications," Mass Spectrom. Rev. **30**(2), 236–267 (2011).
29. H. Z. Castada and S. A. Barringer, "Online, real-time, and direct use of sift-ms to measure garlic breath deodorization: a review," Flavour Fragrance J. **34**(5), 299–306 (2019).

Biomedical Optics EXPRESS

30. R. B. Michalcíková, K. Dryahina, and P. Španel, "Sift-ms quantification of several breath biomarkers of inflammatory bowel disease, ibd: A detailed study of the ion chemistry," Int. J. Mass Spectrom. **396**, 35–41 (2016).
31. D. Milligan, G. Francis, B. Prince, *et al.*, "Demonstration of selected ion flow tube ms detection in the parts per trillion range," Anal. Chem. **79**(6), 2537–2540 (2007).
32. M. Thorpe, D. Hudson, K. Moll, *et al.*, "Cavity-ringdown molecular spectroscopy based on an optical frequency comb at 1.45-1.65μm," Optica **32**(3), 307–309 (2007).
33. M. Weichman, P. Changala, J. Ye, *et al.*, "Broadband molecular spectroscopy with optical frequency combs," J. Mol. Spectrosc. **355**, 66–78 (2019).
34. N. Picqué, T. Hänsch, and W. Theodor, "Frequency comb spectroscopy," Nat. Photonics **13**(3), 146–157 (2019).
35. L. I. Wassenaar, M. Ahmad, P. Aggarwal, *et al.*, "Worldwide proficiency test for routine analysis of δ^2h and δ^{18}o in water by isotope-ratio mass spectrometry and laser absorption spectroscopy," Rapid Commun. Mass Spectrom. **26**(15), 1641–1648 (2012).
36. J. R. Köster, R. Well, B. Tuzson, *et al.*, "Novel laser spectroscopic technique for continuous analysis of n^{2}o isotopomers - application and intercomparison with isotope ratio mass spectrometry," Rapid Commun. Mass Spectrom. **27**(1), 216–222 (2013).
37. E. Kerstel and L. Gianfrani, "Advances in laser-based isotope ratio measurements: selected applications," Appl. Phys. B **92**(3), 439–449 (2008).
38. A. Srivastava, S. E. Long, J. E. Norris, *et al.*, "Comparison of primary laser spectroscopy and mass spectrometry methods for measuring mass concentration of gaseous elemental mercury," Anal. Chem. **93**(2), 1050–1058 (2021).
39. S. Scholten, J. Anstie, N. Herbert, *et al.*, "Complex direct comb spectroscopy with a virtually imaged phased array," Opt. Lett. **41**(6), 1277–1280 (2016).
40. S. Scholten, C. Perrella, J. Anstie, *et al.*, "Number-density measurements of co_2 in real time with an optical frequency comb for high accuracy and precision," Phys. Rev. Appl. **9**(5), 054043 (2018).
41. S. Scholten, C. Perrella, J. Anstie, *et al.*, "Accurate optical number density measurement of $^{12}co_2$ and $^{13}co_2$ with direct frequency comb spectroscopy," Phys. Rev. Appl. **12**(3), 034045 (2019).
42. F. Karim, S. Scholten, C. Perrella, *et al.*, "Ultrahigh-resolution direct-frequency-comb spectrometer," Phys. Rev. Appl. **14**(2), 024087 (2020).
43. F. Adler, M. Thorpe, K. Cossel, *et al.*, "Cavity-enhanced direct frequency comb spectroscopy: Technology and applications," Annu. Rev. Anal. Chem. **3**(1), 175–205 (2010).
44. G. B. Rieker, F. R. Giorgetta, W. C. Swann, *et al.*, "Frequency-comb-based remote sensing of greenhouse gases over kilometer air paths," Optica **1**(5), 290 (2014).
45. L. C. Sinclair, I. Coddington, W. C. Swann, *et al.*, "Operation of an optically coherent frequency comb outside the metrology lab," Opt. Express **22**(6), 6996 (2014).
46. N. Hoghooghi, R. J. Wright, A. S. Makowiecki, *et al.*, "Broadband coherent cavity-enhanced dual-comb spectroscopy," Optica **6**(1), 28 (2019).
47. M. Thorpe and J. Ye, "Cavity-enhanced direct frequency comb spectroscopy: application to human breath analysis," Appl. Phys. B: Lasers Opt. **91**(3-4), 397–414 (2008).
48. Q. Liang, Y. Chan, P. B. Changala, *et al.*, "Ultrasensitive multispecies spectroscopic breath analysis for real-time health monitoring and diagnostics," Proc. Natl. Acad. Sci. **118**(40), e2105063118 (2021).
49. Q. Liang, Y. Chan, J. Toscano, *et al.*, "Breath analysis by ultra-sensitive broadband laser spectroscopy detects sars-cov-2 infection," J. Breath. Res. **17**(3), 036001 (2022).
50. G. Kowzan, D. Charczun, A. Cygan, *et al.*, "Broadband optical cavity mode measurements at hz-level precision with a comb-based vipa spectrometer," Sci. Rep. **9**(1), 8206 (2019).
51. N. Zhu, Z. Song, W. Wang, *et al.*, "Mid-infrared virtually imaged phased array spectrometer with optical frequency comb: fast thermometry over large dynamic range," Meas. Sci. Technol. **34**(12), 125501 (2023).
52. D. Bailey, G. Zhao, and A. Fleisher, "Precision spectroscopy of nitrous oxide isotopocules with a cross-dispersed spectrometer and a mid-infrared frequency comb," Anal. Chem. **92**(20), 13759–13766 (2020).
53. B. Müller and U. Grossniklaus, "Model organisms - a historical perspective," Journal of Proteomics **73**(11), 2054–2063 (2010).
54. J. Nielsen, "Yeast systems biology: Model organism and cell factory," Biotechnol. J. **14**(9), 1 (2019).
55. S. Mohammadi, B. Saberidokht, S. Subramaniam, *et al.*, "Scope and limitations of yeast as a model organism for studying human tissue-specific pathways," BMC Syst. Biol. **9**(1), 96 (2015).
56. D. Botstein, S. A. Chervitz, and J. M. Cherry, "Yeast as a model organism," Science **277**(5330), 1259–1260 (1997).
57. H. Karathia, E. Vilaprinyo, A. Sorribas, *et al.*, "Saccharomyces cerevisiae as a model organism: A comparative study," PLoS One **6**(2), e16015 (2011).
58. R. F P. Ludovico and C. Leao, "Sugar metabolism in yeasts: An overview of aerobic and anaerobic glucose catabolism," in *The Yeast Handbook Biodiversity and Ecophysiology of Yeasts*, C. A. Rosa and G. Peter, eds. (Springer, 2006), chap. 6, pp. 101–123.
59. T. D'Amore, I. Russell, and G. G. Stewart, "Sugar utilization by yeast during fermentation," J. Ind. Microbiol. **4**(4), 315–323 (1989).
60. B. Turcotte, X. B. Liang, F. Robert, *et al.*, "Transcriptional regulation of nonfermentable carbon utilization in budding yeast," FEMS Yeast Research **10**(1), 2–13 (2010).
61. S. Maicas, "The role of yeasts in fermentation processes," Microorganisms **8**(8), 1142 (2020).

Biomedical Optics EXPRESS

62. W. L. Marques, V. Raghavendran, B. U. Stambuk, *et al.*, "Sucrose and saccharomyces cerevisiae: A relationship most sweet," FEMS Yeast Research **16**(1), fov107 (2015).
63. C. Compagno, S. Dashko, and J. Piškur., "Introduction to carbon metabolism in yeast," in *Molecular Mechanisms in Yeast Carbon Metabolism*, J. Piškur and C. Compagno, eds. (Springer, 2014), chap. 1, pp. 1–20.
64. J. A. Barnett and K.-D. Entian, "A history of research on yeasts 9: regulation of sugar metabolism," Yeast **22**(11), 835–894 (2005).
65. T. Pfeiffer and A. Morley, "An evolutionary perspective on the crabtree effect," Frontiers in Molecular Biosciences **1**, 17 (2014).
66. K. Otterstedt, C. Larsson, R. M. Bill, *et al.*, "Switching the mode of metabolism in the yeast saccharomyces cerevisiae," EMBO Rep. **5**(5), 532–537 (2004).
67. S. Freeman, K. Quillin, L. Allison, *et al.*, *Biological Science* (Pearson, 2016), chap. 9, pp. 189–209, 6th ed.
68. C. Verduyn, T. P. L. Zomerdijk, J. P. van Dijken, *et al.*, "Continuous measurement of ethanol production by aerobic yeast suspensions with an enzyme electrode," Appl. Microbiol. Biotechnol. **19**(3), 181–185 (1984).
69. R. H. D. Deken, "The role of yeasts in fermentation processes," Microorganisms **44**, 149–156 (1966).
70. O. Käppelli, "Regulation of carbon metabolism in *Saccharomyces cerevisiae* and related yeasts advances in microbial physiology," Advances in Microbial Physiology **28**, 181–209 (1987).
71. T. Deak, "Environmental factors influencing yeasts," in *The Yeast Handbook Biodiversity and Ecophysiology of Yeasts*, C. A. Rosa and G. Peter, eds. (Springer, 2006), chap. 8, pp. 155–175.
72. I. Gordon, L. Rothman, R. Hargreaves, *et al.*, "The hitran2020 molecular spectroscopic database," J. Quant. Spectrosc. Radiat. Transfer **277**, 107949 (2022).
73. R. R. Gamache, R. L. Hawkins, and L. S. Rothman, "Total internal partition sums in the temperature range 70-3000 k: Atmospheric linear molecules," J. Mol. Spectrosc. **142**(2), 205–219 (1990).
74. H. Alsuhaim, V. Vojisavljevic, and E. Pirogova, "Effects of non-thermal microwave exposures on the proliferation rate of saccharomyces cerevisiae yeast," in *World Congress on Medical Physics and Biomedical Engineering May 26-31, 2012, Beijing, China*, vol. 39 M. Long, ed. (Springer, 2013), pp. 48–51.
75. H. Shafaghat, G. D. Najafpour, P. S. Rezaei, *et al.*, "Optimal growth of saccharomyces cerevisiae (ptcc 24860) on pretreated molasses for the ethanol production: the application of the response surface methodology," Chem. Ind. Chem. Eng. Q. **16**(2), 199–206 (2010).
76. G. Stahl, S. N. B. Salem, L. Chen, *et al.*, "Translational accuracy during exponential, postdiauxic, and stationary growth phases in saccharomyces cerevisiae," Eukaryot. Cell **3**(2), 331–338 (2004).
77. M. W. Ojewumi, A. I. Job, O. S. Taiwo, *et al.*, "Bio-conversion of sweet potato peel waste to bio-ethanol using saccharomyces cerevisiae," Int. J. Pharm. Phytopharm. Res. **8**, 46–54 (2018).
78. P. U. Amadi and M. O. Ifeanacho, "Impact of changes in fermentation time, volume of yeast, and mass of plantain pseudo-stem substrate on the simultaneous saccharification and fermentation potentials of african land snail digestive juice and yeast," J. Genet. Eng. Biotechnol. **14**(2), 289–297 (2016).
79. P. Sroka, P. Satora, T. Tarko, *et al.*, "The influence of yeast immobilization on selected parameters of young meads," J. The Inst. Brew. **123**(2), 289–295 (2017).
80. S. L. Chen and F. Gutmanis, "Carbon dioxide inhibition of yeast growth in biomass production," Biotechnol. Bioeng. **18**(10), 1455–1462 (1976).
81. M. Vidal-Leiria, H. Buckley, and N. van Uden, "Distribution of the maximum temperature for growth among yeasts," Mycologia **71**(3), 493–501 (1979).
82. S. K. Yalcin and Z. Y. Ozbas, "Effects of ph and temperature on growth and glycerol production kinetics of two indigenous wine strains of saccharomyces cerevisiae from turkey," Braz. J. Microbiol. **39**(2), 325–332 (2008).
83. N. V. Uden and A. Madeira-Lopes, "Dependence of the maximum temperature for growth of saccharomyces cerevisiae on nutrient concentration," Arch. Microbiol. **104**(1), 23–28 (1975).
84. W. Wilson, P. Roach, M. Montero, *et al.*, "Regulation of glycogen metabolism in yeast and bacteria," FEMS Microbiol. Rev. **34**(6), 952–985 (2010).
85. L. D. Whigham, D. E. Butz, L. K. Johnson, *et al.*, "Breath carbon stable isotope ratios identify changes in energy balance and substrate utilization in humans," Int. J. Obes. **38**(9), 1248–1250 (2014).
86. O. A. F. Bodamer and D. Halliday, "Uses of stable isotopes in clinical diagnosis and research in the paediatric population," Arch. Dis. childhood **84**(5), 444–448 (2001).
87. G. S. Timmins, "Stable isotope biomarker breath tests for human metabolic and infectious diseases: a review of recent patent literature," Expert Opin. Ther. Pat. **26**(12), 1393–1398 (2016).
88. B. Long, A. Koyfman, and M. A. Vivirito, "Capnography in the emergency department: A review of uses, waveforms, and limitations," Clin. Rev. Emerg. Med. **53**(6), 829–842 (2017).
89. M. Hussin, M. Ismail, and M. Ahmad, "Air-conditioned university laboratories: Comparing CO_2 measurement for centralized and split-unit systems," J. King Saud Univ. Eng. Sci. **29**(2), 191–201 (2017).
90. V. Savarino, S. Vigneri, and G. Celle, "The 13c urea breath test in the diagnosis of helicobacter pylori infection," Gut **45**(Supplement 1), 18–22 (1999).
91. J. P. Gisbert and J. M. Pajares, "Review article: ^{1}3c-urea breath test in the diagnosis of helicobacter pylori infection - a critical review," Aliment. Pharmacol. Ther. **20**(10), 1001–1017 (2004).
92. F. Adler, P. Maslowski, A. Foltynowicz, *et al.*, "Mid-infrared fourier transform spectroscopy with a broadband frequency comb," Optica **18**(21), 21861–21872 (2010).

Biomedical Optics EXPRESS

93. D. F. Swinehart, "The Beer-Lambert law," J. Chem. Educ. **39**(7), 333–335 (1962).
94. J. Hodgkinson and R. P. Tatam, "Optical gas sensing: a review," Meas. Sci. Technol. **24**(1), 012004 (2013).